3 Nonlinear magneto-optics - theoretical aspects

The aim of this chapter is to introduce the nonlinear optics in general, and the nonlinear magneto-optical effects, in particular. As a representative of the latter ones is the magnetization-induced second harmonic generation (MSHG), that is the tool of choice employed in the present work. Here, the MSHG is used as a method of investigation of ferromagnetic materials since it has a non-invasive and nondestructive optical character and it exhibits high surface and interface sensitivity. Moreover, due to its symmetry with respect to magnetization reversal, provides simultaneously information about the electron/lattice dynamics as well as spin dynamics.
The chapter is structured as follows: after a brief introduction to nonlinear optics presented in the first section, a more detailed description regarding the second harmonic generation process is developed in the next part. The last two sections focus on the origin of the linear and nonlinear magneto-optical effects and to the description of the MSHG formalism involved in determining the statical and dynamical properties of ferromagnetic metals.

3.1 Nonlinear optics

The field of the nonlinear optics was growing with the laser development. One of the first experiments in which the generation of second harmonic light (in a quartz glass) was demonstrated [96], took place shortly after the discovery of the laser by Maiman in 1960. This fact points out the necessity of having high incident optical intensities involved in order to produce efficient nonlinear processes. Such high electromagnetic field strengths (intensity is the square of electric field) are achievable, for instance, by focussing an ultrashort laser pulse that carries high peak power.

The *optical response* of a medium to an incident electromagnetic wave $\mathbf{E}(\mathbf{r},\mathrm{t})$ is described by the induced electrical polarization $\mathbf{P}(\mathbf{r},\mathrm{t})$. Subsequently, the medium response perturbs the propagation of the optical wave, this mutual dependence giving rise to a richness of optical phenomena like linear and nonlinear optical reflection, linear transmission etc. These are used as investigation tools of optical and electronic properties of materials, just to mention a few potential applications.

Starting from Maxwell equations, one can deduce the optical wave equation for the propagation of the electric field $\mathbf{E}(\mathbf{r},t)$ through a medium under the following form [97]:

$$\nabla \times \nabla \times \mathbf{E}(\mathbf{r},t) + \frac{1}{c^2}\frac{\partial^2}{\partial t^2}\mathbf{E}(\mathbf{r},t) = -\frac{4\pi}{c^2}\frac{\partial^2}{\partial t^2}\mathbf{P}(\mathbf{r},t) \tag{3.1}$$

The wave equation describes the *optical response* of a medium being subject to an incoming electromagnetic field. In the right-hand part of eq. 3.1, the time variation of polarization acts as a source term for the emitted waves, which in the classical physics picture is the equivalent of an oscillating dipole that radiates light.
Depending on the strength of the incident field, the polarization consists of two contributions, a linear and a nonlinear one:

$$\mathbf{P}(\mathbf{r},t) = \mathbf{P}^{L}(\mathbf{r},t) + \mathbf{P}^{NL}(\mathbf{r},t) \tag{3.2}$$

The linear response of the medium is described by [97]:

$$\mathbf{P}^{L}(\mathbf{r},t) = \int_{0}^{+\infty} dt_1 \int_{-\infty}^{+\infty} \varepsilon_0 \chi^{(1)}(\mathbf{r}-\mathbf{r}_1, t-t_1)\mathbf{E}(\mathbf{r}_1,t_1)d\mathbf{r}_1 \tag{3.3}$$

where ε_0 is the dielectric constant in vacuum and the $\chi^{(1)}$ is the linear susceptibility tensor. Since the medium response is described by a tensor, has not necessarily the same directionality as the incoming electric field *i.e.* can be optically anisotropic.
For stronger optical fields higher orders terms in polarization expression become non-negligible and should be take into account. Expanding the polarization in power series of electric field, one obtains:

$$\mathbf{P}^{(n)}(\mathbf{r},t) = \int_{0}^{+\infty} dt_1..dt_n \int_{-\infty}^{+\infty} \varepsilon_0 \chi^{(n)}(\mathbf{r}-\mathbf{r}_1,..,\mathbf{r}-\mathbf{r}_n, t-t_1,..,t-t_n)\mathbf{E}(\mathbf{r}_1,t_1)..\mathbf{E}(\mathbf{r}_n,t_n)d\mathbf{r}_1..d\mathbf{r}_n \tag{3.4}$$

with the total polarization being:

$$\mathbf{P}(\mathbf{r},t) = \sum_{n} \mathbf{P}^{(n)}(\mathbf{r},t) \tag{3.5}$$

Here, the n-th order polarization is determined by the n-th order nonlinear susceptibility tensor and the n-th power of the incident electric field. We notice that the nonlinear susceptibility tensor $\chi^{(n)}$ has a nonlocal and a non-instantaneous character. In other words, the induced polarization is not a local (point-like) characteristic and is not produced simultaneously when the incident light reached the medium under consideration. The causality principle is fulfilled since in equations 3.3 and 3.4 one integrates over time between 0 and infinity which means that one takes into account only past values of $\mathbf{E}$ vector but not the future ones *i.e.* $t - t_n > 0$. The non-locality aspect, which is important in the context of bulk contributions to the SHG process, will be addressed later in this section.

If one assumes an incident monochromatic electromagnetic wave and calculates the Fourier transformation of equation 3.5, one ends up with the total polarization in frequency space, which in the dipole approximation reads:

$$\mathbf{P}(\omega) = \mathbf{P}^{(1)}(\omega) + \mathbf{P}^{(2)}(2\omega = \omega_1 + \omega_2) + \mathbf{P}^{(3)}(3\omega = \omega_1 + \omega_2 + \omega_3) + ... \tag{3.6}$$

which is equivalent with:

$$\mathbf{P} = \varepsilon_0[\chi^{(1)}(\omega)\mathbf{E}(\omega) + \chi^{(2)}(\omega = \omega_1 + \omega_2)\mathbf{E}(\omega_1)\mathbf{E}(\omega_2) + ...] \tag{3.7}$$

The first term in the above equation is the source for linear optical processes like reflection and absorption whereas the next term describes second-order processes as SHG, SFG and so on. Examples of second and higher order nonlinearities described by the eq. 3.7 are given in the table 3.1, all processes being listed with the corresponding nonlinear tensors.

Nonlinear optical process	$\chi^{(2)}$
Second harmonic generation	$\chi^{(2)}(2\omega = \omega + \omega)$
Sum-frequency generation	$\chi^{(2)}(\omega = \omega_1 + \omega_2)$
Difference-frequency generation	$\chi^{(2)}(\omega = \omega_1 - \omega_2)$
Optical rectification	$\chi^{(2)}(0 = \omega - \omega)$
Nonlinear optical process	$\chi^{(3)}$
Third harmonic generation	$\chi^{(3)}(3\omega = \omega + \omega + \omega)$
Four-wave mixing	$\chi^{(3)}(\omega = \omega_1 + \omega_2 + \omega_3)$
Optical Kerr effect	$\chi^{(3)}(\omega = \omega + \omega_1 - \omega_1)$
Nonlinear optical process	$\chi^{(n)}$
High-harmonic generation	$\chi^{(n)}(n\omega = \omega + \omega + .. + (n-1)\omega)$

Table 3.1: Examples of second-, third- and higher-order nonlinear optical processes together with the susceptibility tensors that describe them.

3.2 Second Harmonic Generation (SHG)

As an example for a second order nonlinear optical processes, we take the case of second harmonic generation, being the main tool of investigation in this work. Actually, the SHG is a degenerate case of sum-frequency generation (SFG) *i.e.* $\omega = \omega_1 + \omega_2$ with both incident photons having the same frequency $\omega_1 = \omega_2 = \omega$. Thus, one can write, within electric-dipole approximation[1], the nonlinear polarization governing the SHG process as :

$$\mathbf{P}^{(2)}(2\omega) = \varepsilon_0 \chi^{(2)}(2\omega)\mathbf{E}(\omega)\mathbf{E}(\omega) \tag{3.8}$$

In a cartesian coordinate system, the polarization can be express as:

$$\mathbf{P}_i^{(2)}(2\omega) = \varepsilon_0 \chi_{ijk}^{(2)}(2\omega)\mathbf{E}_j(\omega)\mathbf{E}_k(\omega) \tag{3.9}$$

where the subscripts *i, j, k* run over the cartesian coordinates *x, y,* and *z*. The above relation shows that the i-th component of the second-order polarization is induced by the j-th and k-th components of the incoming electric field at the fundamental frequency.

3.2.1 SHG - microscopic formalism

Microscopically the second-harmonic generation process is described by a nonlinear susceptibility tensor that can be deduced within the density matrix formalism of quantum mechanics and has the following expression [97]:

$$\chi_{ijk}(2\omega) = -Ne^3 \int d\mathbf{k}\{\frac{<1,\mathbf{k}|r_i|3,\mathbf{k}><3,\mathbf{k}|r_j|2,\mathbf{k}><2,\mathbf{k}|r_k|1,\mathbf{k}>}{[2\hbar\omega - E_{31}(\mathbf{k}) - i\hbar\Gamma_{31}][\hbar\omega - E_{21}(\mathbf{k}) - i\hbar\Gamma_{21}]} f_1(\mathbf{k}) + \chi^{NR}\}, \tag{3.10}$$

[1] Within electric-dipole approximation one takes into account just the contribution from the oscillating electric dipoles induced by the incident electromagnetic field. The contributions from the magnetic field part of the light wave and from the electric quadrupoles are much weaker and are usually neglected.

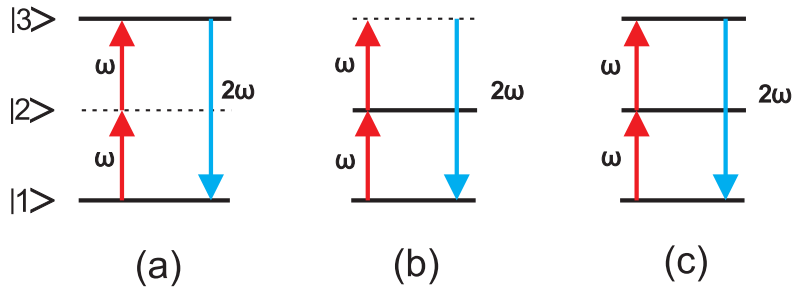

Figure 3.1: Schematic description of the SHG process showing the involved optical transitions at fundamental frequency ω and at the second-harmonic frequency 2ω among real (thick line) and virtual levels (dashed line). The initial, intermediate and final energetic levels are denoted by $|1\rangle$, $|2\rangle$, and $|3\rangle$, respectively.

where the optical transitions take place among $|1\rangle$,$|2\rangle$ and $|3\rangle$ states, which denote the initial, intermediate and the final state, respectively. The density of electrons per volume was noted by Ne^3 with the Fermi distribution factor being $f_1(\mathbf{k})$ for the state $|1, \mathbf{k}>$ with the electron wave vector $\mathbf{k}$. The cartesian coordinate operator is $r_{i,j,k}$ and the $\hbar\Gamma$ is the linewidth of the transitions between two electronic states. The non-resonant susceptibility terms are denoted by χ^{NR}.
As it can be observed, just the resonant part of the nonlinear tensor is written explicitly, as is the relevant part for our future discussions. It is clear that the SHG can be resonantly enhanced if the photon energies of the involved transitions match either the energetic interval between states $|1\rangle$ and $|2\rangle$ at fundamental frequency or between $|1\rangle$ and $|3\rangle$ at $2\hbar\omega$. These two situations are illustrated in the figure 3.1 b,c.

For a better illustration of the resonance condition that might appear in a SHG process, we have simulated the magnitude of the susceptibility tensor and of the corresponding phase for a resonance situation at $2\hbar\omega$ and $\hbar\omega$ according to eq. 3.10 (for simplicity without matrix elements and the Fermi function). At this point the phase of the second-order susceptibility can be understood as the phase of a complex number: $\chi^{(2)} = |\chi^{(2)}| \cdot e^{i\varphi}$. The result of the computation is displayed in the figure 3.2. Here we observe a sharp increase of $|\chi^{(2)}|$ and a 180° phase change as the photon energy is crossing the resonance at the fundamental $\hbar\omega$ or at the second-harmonic $2\hbar\omega$ photon energy. Thus, in a SHG measurement one can identify the presence of a SHG resonance by monitoring the behavior of the SHG signal (SHG intensity scales with the magnitude of $|\chi^{(2)}|$, see eq. 3.18) and of the phase. The phase can be retrieved in a separate measurement that is described in detail in chapter 5. The values of involved parameters in the simulation are Γ_{31}=1/20 and Γ_{21}=1/40.

3.2.2 SHG - symmetry considerations

As we have seen above the second-order nonlinear effects are governed by a third-rank susceptibility tensor $\chi^{(2)}$. It consists of 27 independent components and because generally is a complex number the total number of components which should be take into account

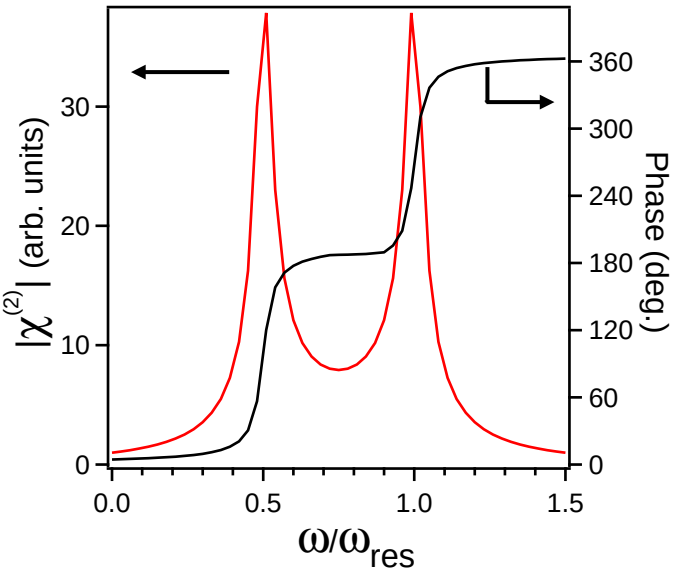

Figure 3.2: The calculated magnitude of the second-order susceptibility tensor and of the corresponding phase change in the case of a double resonance with ω_{res} equal to 2ω and ω photon frequencies, according to the first term in the formula 3.10. Note the 180° phase change for each of the encountered resonance.

is 54. This fact makes the evaluation of the SHG response of a certain medium in a quantitative manner a difficult task. It is the symmetry of the involved system which reduces the number of non-zero tensor components and thus simplifying the computation of the SH signal. A general symmetry framework is developed on the base of Neumann's principle [98], which states that the symmetry exhibited by a certain system is possessed by every physical property of that system. In other words, the system properties should be invariable with regard to the symmetry operations that define the space group of the system.
As an example, let us take the case of centrosymmetric medium *i.e.* a medium that posses inversion symmetry. This type of medium symmetry is the widest met in nature and is also relevant for our further considerations. Now one can write eq. 3.7 in a compressed manner for the case of a SHG process:

$$\mathbf{P} = \varepsilon_0[\chi^{(1)}\mathbf{E} + \chi^{(2)}\mathbf{EE} + \chi^{(3)}\mathbf{EEE} + ...] \tag{3.11}$$

Under the inversion symmetry operation the **P** and **E** should change the sign since both are *polar* vectors. Under the effect of the inversion operation relation 2.11 becomes :

$$\text{-}\mathbf{P} = \varepsilon_0[-\chi^{(1)}\mathbf{E} + \chi^{(2)}\mathbf{EE} - \chi^{(3)}\mathbf{EEE} + ...] \tag{3.12}$$

The above equations are both valid when $\chi^{(2)}$=0. That means, in general, for these type of materials the even order susceptibility tensors are 0, within the electric-dipole approximation. However, there are regions of the centrosymmetric materials where the

inversion symmetry is broken. For instance, at the surface of a medium or at the interface between two materials where locally the inversion symmetry is lifted.
Therefore, for centrosymmetric materials and within the electric-dipole approximation, the SHG process has an intrinsic sensitivity to surfaces and interfaces where the inversion symmetry is broken.

Coming back to our discussion regarding the number of non-vanishing independent components of $\chi^{(2)}$, for the particular case of the SHG process, owing to the identical frequency of involved photons the total components number is reduced from 27 to 18. This is determined by the identity $\chi^{(2)}_{ijk} \equiv \chi^{(2)}_{ikj}$. Thus, one can write the SHG nonlinear polarization expression under the following form:

$$\begin{pmatrix} P_x \\ P_y \\ P_z \end{pmatrix} = \begin{pmatrix} \chi_{xxx} & \chi_{xyy} & \chi_{xzz} & \chi_{xyz} & \chi_{xxz} & \chi_{xxy} \\ \chi_{yxx} & \chi_{yyy} & \chi_{yzz} & \chi_{yyz} & \chi_{yxz} & \chi_{yxy} \\ \chi_{zxx} & \chi_{zyy} & \chi_{zzz} & \chi_{zyz} & \chi_{zxz} & \chi_{zxy} \end{pmatrix} \begin{pmatrix} E_x E_x \\ E_y E_y \\ E_z E_z \\ 2E_y E_z \\ 2E_x E_z \\ 2E_x E_y \end{pmatrix} \tag{3.13}$$

The elements of $\chi^{(2)}$ tensor can be further reduced by taking into account the particular symmetry of the system. Moreover, choosing a certain crystallographic orientation of the surface and experimental geometry (light polarization, azimuthal orientation of the sample) the number of tensor components that contributes to the generation of SH signal is further decreased.

Since we are interested in the hcp(0001) surface, in the following the calculation of tensor components for this particular surface orientation is presented. The deduction of the tensor components is straightforward since one has to check the invariability of these components under each symmetry operation of the group that defines the symmetry of the system. This can be written under the following form:

$$\chi_{ijk} = \sum_{i\prime j\prime k\prime} T_{ii\prime} T_{jj\prime} T_{kk\prime} \chi_{i\prime j\prime k\prime} \tag{3.14}$$

For instance, the transformation matrix T has the following elements for the case of rotation with the angle Ψ along z axis (normal to the surface): $\begin{pmatrix} \cos\Psi & \sin\Psi & 0 \\ -\sin\Psi & \cos\Psi & 0 \\ 0 & 0 & 1 \end{pmatrix}$
The hcp (hexagonally closed-packed) unit cell of bulk gadolinium has a D_{6h} symmetry whereas the (0001) surface posses an *effective* C_{6v} symmetry. By surface here is meant the first two atomic layers that form the stacking sequence along c axis in the hcp unit cell. At the first sight, considering the first two layers at the Gd(0001) surface one ends up with a C_{3v} symmetry. However, an effective C_{6v} symmetry of the Gd(0001) surface has been revealed by a combined X-ray photoelectron diffraction (XPD) and LEED study [99]. Also we have checked this issue by applying an additional rotation operation of 60° to the tensor components obtained for C_{3v} symmetry. Both even and odd tensor components reproduce the tensor elements of C_{6v} symmetry. Therefore, in our further consideration we take the Gd(0001) surface as having a C_{6v} symmetry.

	p-P	p-S	s-P	s-S	mix-P	mix-S
even	zzz,zxx,xzx	-	zyy	-	zzz,zxx,xzx,zyy	yzy
odd (**M**‖y)	xxx,xzz,zzx	-	xyy	-	xxx,xyy,xzz,zzx	yxy
odd (**M**‖x)	-	yxx,yzz	-	yyy	xxy,zzy	yxx,yyy,yzz
odd (**M**‖z)	-	yxz	-	-	xzy,zxy	yxz

Table 3.2: List of the allowed tensor components for a C_{6v} surface symmetry for various polarization geometries and magnetization directions. For simplicity we denote the tensor components just by their indices.

Applying relation 3.14 for a system with a C_{6v} symmetry one ends up with the allowed tensor components for hcp(0001) surface:

$$\chi_{xxz} = \chi_{yyz}; \quad \chi_{zxx} = \chi_{zyy}; \quad \chi_{zzz}$$

In the presence of magnetization the symmetry of the system is lowered but the inversion symmetry is not lifted since the magnetization is an *axial* vector *i.e.* does not change the sign under inversion symmetry. Thus, the surface and interface sensitivity is not lost for a magnetized system but the expression for the $\chi^{(2)}$ tensor becomes more complicated since one has to deal with a higher number of components. For the transversal geometry (see figure 3.4) used in this work, magnetization lies in the plane of the sample which lowers the symmetry from C_{6v} to C_2. Considering the magnetization direction parallel to y axis and the optical incidence plane determined by x and z axes, the additional allowed tensor components are:

$$\begin{pmatrix} \chi_{xxx}^{odd} & \chi_{xyy}^{odd} & \chi_{xzz}^{odd} & 0 & \chi_{xxz}^{even} & 0 \\ 0 & 0 & 0 & \chi_{yyz}^{even} & 0 & \chi_{yyx}^{odd} \\ \chi_{zxx}^{even} & \chi_{zyy}^{even} & \chi_{zzz}^{even} & 0 & \chi_{zzx}^{odd} & 0 \end{pmatrix} \tag{3.15}$$

Some of the new tensor components behave odd with respect to magnetization reversal *i.e.* $\chi^{(2)}(\mathbf{M}) = -\chi^{(2)}(-\mathbf{M})$ while some do not change the sign $\chi^{(2)}(\mathbf{M}) = \chi^{(2)}(-\mathbf{M})$. From now on, the latter ones will be denoted under *even* tensor components while the former ones under *odd* tensor components. The even and odd tensor components of $\chi^{(2)}$ for a C_{6v} surface symmetry as a function of magnetization orientation and polarization geometry are listed in the table 3.2.

The effect of the even and odd tensor components on the SHG process can be readily seen by considering two cases with different magnetization direction: transversal and longitudinal (see figure 3.4) for a s-polarized incident light. According to table 3.2 for transversal geometry we have two tensor components: one even χ_{zyy} and one odd χ_{xyy} *i.e.* for a s-polarized fundamental. Both of them give a p-polarized SHG output. For longitudinal geometry we have the same even component χ_{zyy} but an odd term χ_{yyy}, which means a p-polarized SHG from the even term and a s-polarized SHG from the odd term. Thus, upon magnetization reversal, one obtains in the transversal geometry a change in the SHG intensity whereas for the longitudinal configuration the effect is the rotation of the SHG polarization.

One way to obtain the even and odd components is to expand susceptibility tensor in powers of magnetization **M**:

$$\chi^{(2)}(\mathbf{M}) = \chi^{(2)}(0) + \frac{\partial \chi^{(2)}}{\partial \mathbf{M}}\mathbf{M} + ... \tag{3.16}$$

The first term in right-hand side represents the even tensor component and the next term in the development is the odd term that is *proportional to the magnetization*. Based on these considerations, one can write an effective tensor that describes the total SHG response from a magnetized material under the form:

$$\chi^{eff}(\mathbf{M}) = \chi^{even}_{eff} + \chi^{odd}_{eff} \tag{3.17}$$

where χ^{even}_{eff} and χ^{odd}_{eff} are linear combinations of tensor components and the corresponding Fresnel factors that are allowed by system symmetry and experimental geometry. Such a simplification is valid when the Fresnel coefficients f_{ijk} might be considered constants and when only the relative changes in $\chi^{(2)}_{ijk}$ are relevant. Thus one can write the expression for the SH intensity as:

$$I(2\omega) = |\sum_{i,j,k} f_{ijk}\chi^{(2)}_{eff}|^2 I(\omega)^2 \tag{3.18}$$

Bulk contributions to $\mathbf{P}^{(2)}(2\omega)$

It should be noted, that at the surface one can encounter high electric field gradients due to the boundary existence, that can add higher order contributions to the second order nonlinear polarization. These contributions have a non-local character and are described by a fourth-rank tensor which is allowed in the bulk of centrosymmetric materials. Therefore, beside probing the surface/interface one might have also components to the SHG yield that contain information about the bulk of the investigated system. Moreover, when the volume of the studied system is considerable the small bulk contribution might add together and thus having a significant contribution to the total SHG response. In order to account for the bulk contributions to the SHG response, the equation 3.8 can be written now in the following form:

$$\mathbf{P}^{(2)}(2\omega) = \mathbf{P}^{D}(2\omega) + \mathbf{P}^{Q}(2\omega) = \varepsilon_0\chi^{(2)}(2\omega)\mathbf{E}(\omega)\mathbf{E}(\omega) + \varepsilon_0\chi^{(Q)}\mathbf{E}(\omega)\nabla\mathbf{E}(\omega) \tag{3.19}$$

Here, the D and Q superscripts stand for dipole and quadrupole contributions, respectively. In general, the non-local component of total polarization consists of electric quadrupoles and magnetic dipoles sources which according to [97] are described by:

$$\mathbf{P}^{Q}(2\omega) = \alpha[\mathbf{E}(\omega)\nabla]\mathbf{E}(\omega) + \beta\mathbf{E}(\omega)[\nabla\mathbf{E}(\omega)] + i\left(\frac{2\omega}{c}\right)\gamma[\mathbf{E}(\omega)\times\mathbf{B}(\omega)] \tag{3.20}$$

where α, β and γ are phenomenological constants. The first two terms in equation have electric quadrupole character whereas the last term describes the magnetic dipole contribution.
In the electric-dipole approximation one takes into account just the local contributions

to the total induced polarization of the medium. Experimentally, it is difficult to distinguish between surface and bulk contributions to the total SHG response from a certain material. However, there are reports [100, 101] in literature where has been shown that under special circumstances (employing certain experimental geometries) one can separate these contributions. Since during this work we never observed a measurable bulk (*i.e.* nonlocal) contribution to the SHG response of the investigated systems of Gd(0001) and Y(0001) films on W(110) substrate, we neglect this in our further considerations. It has been shown [44], that in the case of second harmonic generation the local and nonlocal contributions are of comparable strength if there is a non-resonant transition involved. We will see later for the case of gadolinium that the SHG response is resonantly enhanced via the surface state components [102], a fact that makes us more confident in excluding any bulk contribution to the total SHG yield for this particular system.

3.2.3 SHG radiation depth

An interesting point is the spatial extent over which the SH signal is radiated. A general answer to this issue is the region over which the bulk electronic density exhibits a variation due to the presence of a surface (or interface) that produces a perturbation of the translational symmetry along the z axis *i.e.* normal to the surface. Thus, from symmetry considerations only, a quantitative information cannot be retrieved.

Another way of viewing these variations of the charge density at the surface is qualitatively reproduced in the framework of jellium model [103] by the so called Friedel oscillations. In this model the discrete positions of the ionic charges are replaced by a continuous positive background and the electronic density exhibits a damped oscillatory behavior inside the jellium in order to screen the background. The damping length is proportional to the background density. Usually the charge density of jellium is specified by the corresponding Wigner-Seitz radius in atomic units. For the case of Gd, the Wigner-Seitz cell radius is r_s is 3.762 a.u. [105] (the inverse value of r_s denotes the background density) and therefore the source of SHG in this case is restricted within two atomic layers (one Gd layer is 2.89 Å).

This link between the jellium model and SH polarization is illustrated in the figure 3.3, which displays the case of a metal with r_s=4 (*i.e.* close to Gd value) and consequently a large distance over which the electronic density oscillates. Here are depicted the calculated electronic density (determines the linear optical response) and the second-order polarization produced by an electric field normal to the surface. What is interesting here is the spatial distribution of the second harmonic polarization P_2(z): the dominant contribution to P_2(z) comes from a surface layer as thin as ≈4Å (accounting for both sides of the surface) and its maximum lies in the vacuum region where the equilibrium electron density decays exponentially. Thus we come to the same result as above that for Gd with r_s=3.762 a.u. the SHG source is located within a region of around two atomic layers. We have to be aware that jellium model is just a simple approximation of the real electronic structure at the surface of metals. However, it can give an important insight about the spatial extent that contributes to the generation of SH radiation.

Beside its intrinsic surface sensitivity derived from symmetry constraints, SHG is particular sensitive to electronic structure at the surface *e.g.* surface states [106], interface

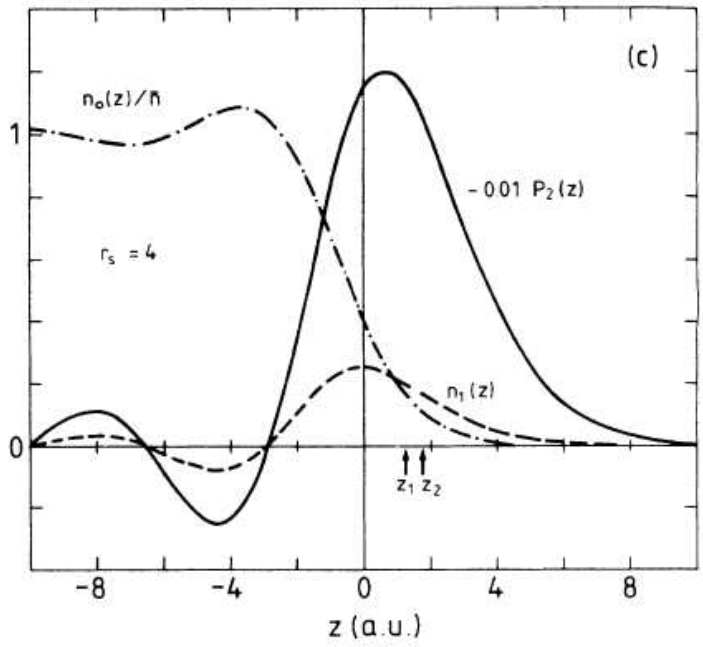

Figure 3.3: Illustration of the spatial distributions of the second harmonic polarization (solid line) and first order electronic polarization (dashed line) produced by an electric field at a metal surface (with r_s=4), calculated within a semi-infinite jellium model. The dashed-dotted line represents the normalized electronic density in equilibrium and the z_1 and z_2 indicate the centroid positions of n_1(z)and P_2(z), respectively. From [104].

states [107] and quantum-well states [108]. The sensitivity is furthermore increased if the optical transitions involved in the SHG process are resonant. This brings us to the case of Gd(0001) surface, which exhibits a d_{z^2}-like surface state that is localized in the top-most atomic layer (89% of the surface state charge density is located in the first atomic layer [27]). We will see in chapter 5 that at the Gd(0001) surface the SHG process is resonantly enhanced via the surface state (see figure 5.11). Thus we can say that for the case of Gd(0001) surface the SHG process is extremely surface sensitive, probing most likely the first two atomic layers (accounting for the charge gradient of the surface state). This arises partially from the common symmetry restriction (within electric-dipole approximation) of the SHG source at the surface, and due to the presence of the surface state via which the SHG process evolves resonantly enhanced.

3.2.4 SHG - macroscopic formalism

For a quantitative evaluation of the SHG response of a certain material one can use the phenomenological formalism developed by Sipe *et al.* [109]. Following their approach one can compute the second-harmonic field using as input parameters the Fresnel coefficients for fundamental $\mathbf{f}(\omega)$ and SH frequencies $\mathbf{F}(2\omega)$, the susceptibility tensor $\chi^{(2)}$, the effective depth over which SHG is radiated ζ and the incident laser intensity $|\mathbf{E}(\omega)|^2$. The condensed

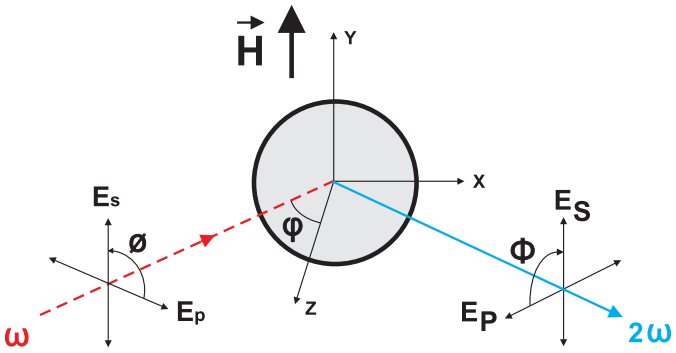

Figure 3.4: Experimental configuration of the SHG process in reflection employed in this work. The fundamental and second harmonic beams are depicted by the dashed and solid lines, respectively, while their polarization orientation is described by ϕ (fundamental) and Φ (second harmonic) angles. φ is the angle of incidence and the external magnetic field **H** sets the magnetization orientation of the system and determines the transversal magneto-optical geometry.

formulation of this expression is given as [110, 44]:

$$\mathbf{E}(2\omega) = \frac{2i\omega}{c}\mathbf{F}(2\omega)\chi^{(2)}\mathbf{f}(\omega)|\mathbf{E}(\omega)|^2\zeta \tag{3.21}$$

The Frenel coefficients are given by:

$$\mathbf{F}(2\omega) = \begin{pmatrix} A_p F_c \cos\Phi \\ A_s \sin\Phi \\ A_p N^2 F_s \cos\Phi \end{pmatrix}; \quad \mathbf{f}(\omega) = \begin{pmatrix} f_c^2 t_p^2 \cos^2\phi \\ t_s^2 \sin^2\phi \\ f_s^2 t_p^2 \cos^2\phi \\ 2 f_s t_p t_s \cos\phi \sin\phi \\ 2 f_c f_s t_p^2 \cos^2\phi \\ 2 f_c t_p t_s \cos\phi \sin\phi \end{pmatrix} \tag{3.22}$$

for the second harmonic and fundamental radiation, respectively. In the above relations the following contracted notation was used:

$$\begin{aligned} f_s &= \frac{sin\varphi}{n(\omega)}, \quad f_c = \sqrt{1 - f_s^2}, \quad t_p = \frac{2\cos\varphi}{n(\omega)\cos\varphi + f_c} \\ t_s &= \frac{2\cos\varphi}{n(\omega) f_c + \cos\varphi}, \quad A_{p/s} = \frac{2\pi T_{p/s}}{\cos\varphi}, \quad N = n(2\omega) \end{aligned} \tag{3.23}$$

where ϕ and Φ denotes the polarization direction for fundamental and second harmonic, respectively (0° for p polarization and 90° for s polarization, see figure 3.4). The lower-case letters describe the quantities at the fundamental frequency whereas capital letters denotes SH related quantities. The angle of incidence is denoted by φ. N and n are the refractive indexes at second-harmonic and fundamental frequency, respectively, $A_{p/s}$ denotes the amplitude of the output SHG for p and s polarized light, $t_{p/s}$ the transmission

coefficients for p and s polarized light, while f_s and f_c represent the projection of the fundamental wavevector on the coordinate system of the sample.

The Fresnel coefficients reflect the linear optical response of the medium at the fundamental and the second-harmonic frequencies, and enter in the SH field formula (and consequently in the SHG intensity) as multiplying factors. This fact is useful since one can increase the SHG yield by choosing the optimal geometry (angle of incidence, wavelength). On the other hand, the fact that the SH field (eq. 3.21) depends on the optical properties of the system at both, SH and fundamental frequency, makes a straightforward interpretation of the SHG response, sometimes, to be difficult. Thus, one should be aware of this fact when trying to obtain quantitative information from the SHG transients in general [111].

From eq.3.21 we have seen that the SH field is proportional to the square of the incident electric field, which gives the same square dependence between the SH $I_{2\omega}$ and the fundamental I_ω intensities. It is of interest here to see what are the experimental parameters that influence the SHG intensity. The SHG intensity is given by:

$$I_{2\omega} \propto \int |\chi^{(2)}| I_\omega^2(t) dt \propto \frac{(E_p/A)^2}{\tau} \tag{3.24}$$

where E_p, A, τ are the pulse energy, laser focus area, and pulse duration respectively. We notice that the SHG signal is material dependent through $\chi^{(2)}$ and it can be optimized by varying one or more parameters that enter in the above equation.

3.3 Magneto-Optics

3.3.1 Linear magneto-optics

The interaction between the light and matter, with the latter one being magnetized - either under the influence of an external magnetic field or showing a spontaneous magnetization - is described in the framework of magneto-optics. Assuming moderate level of incident optical intensities the response of the medium is a linear one (see previous section). The magneto-optical effects manifest themselves as a change in the state of polarization and/or intensity upon light reflection or transmission from magnetized material. In reflection this effect is known as magneto-optical Kerr effect (MOKE), and in transmission under Faraday effect. Both these phenomena resemble similar features, namely are proportional to the magnetization and scale with the thickness of the medium under investigation .

Classically, the MOKE effect can be explained by the action of the Lorentz force on the electrons excited by the incident electromagnetic wave. Although this picture has for sure a high pedagogical usefulness, it does not account for the reality since one needs magnetic fields in order of 10^4 tesla to obtain the observed amplitude of the MOKE signal.
Macroscopically, in a phenomenological approach, the dielectric tensor that describes the optical response of the medium (optically isotropic) can be written as:

$$\varepsilon(\omega) = \begin{pmatrix} \varepsilon_{xx} & 0 & 0 \\ 0 & \varepsilon_{xx} & 0 \\ 0 & 0 & \varepsilon_{xx} \end{pmatrix} \tag{3.25}$$

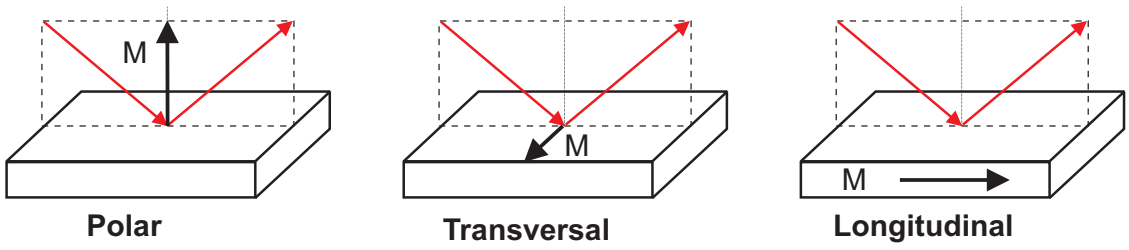

Figure 3.5: Experimental geometries for linear and nonlinear magneto-optics that are defined by the orientation of magnetization **M** direction with respect to the optical incidence plane (dashed rectangle) and the sample. For the polar case the magnetization is perpendicular to the sample surface and in the plane of incidence, for transversal geometry the **M** vector lies in the plane of the sample and perpendicular to the plane of incidence while for the longitudinal situation **M** is parallel with the plane of incidence and the sample surface.

In the presence of magnetization the medium becomes optically anisotropic, the effects induced by the presence of magnetization being described by the off-diagonal tensor components. These ones fulfill the Onsager identity [112] which illustrates the breaking of the time-reversal symmetry in the presence of magnetization:

$$\varepsilon_{ij}(\mathbf{M}) = -\varepsilon_{ij}(-\mathbf{M})$$

Taking this expression into account the dielectric tensor for a magnetized medium becomes:

$$\varepsilon(\omega) = \begin{pmatrix} \varepsilon_{xx} & \varepsilon_{xy} & -\varepsilon_{xz} \\ -\varepsilon_{xy} & \varepsilon_{xx} & \varepsilon_{yz} \\ \varepsilon_{xz} & -\varepsilon_{yz} & \varepsilon_{xx} \end{pmatrix} \tag{3.26}$$

In eq. 3.26 the formula of the dielectric tensor is deduced for the general case when the magnetization has an arbitrary orientation.
As for the second-order susceptibility, expanding ε_{ij} in powers of **M** one obtains:

$$\varepsilon_{ij}(\mathbf{M}) = \varepsilon_{ij}(0) + \frac{\partial \varepsilon_{ij}}{\partial \mathbf{M}}\mathbf{M} \tag{3.27}$$

where the part independent of magnetization (in a first approximation) denotes the diagonal components of the dielectric tensor while the part proportional with magnetization determines the antisymmetric off-diagonal tensor components in equation 3.26.

Until now we have seen that the MO effects are due to the off-diagonal components of the dielectric tensor. But the question is what is the physical picture behind these effects or how the magneto-optics comes about? For sake of simplicity let us follow the Kerr effect scenario: the incident linearly polarized light can be described as a superposition of left and right circularly polarized components with equal amplitudes. As the light travels through the magnetized medium, its constituent parts will "see" different medium with different refractive indexes. This will result, first, in different propagating velocities and implicitly there will be a phase shift between the two modes which produces the rotation of the polarization plane. Second, different absorption rates for the two circularly polarized

waves will change their relative amplitudes and modify the polarization state from linear to elliptical. Their combined effect will produce an elliptically polarized output radiation with the polarization plane rotated with respect to the incident wave polarization axis.

These two effects are quantified by Kerr ellipticity ε_K and rotation θ_K contributions to the complex Kerr angle: $\Theta_K = \theta_k + i\varepsilon_K$. Writing these quantities in terms of dielectric tensor components, one obtains *e.g.* for a magnetized medium in the polar geometry ($\vec{M} \parallel z$):

$$\Theta_K \sim \frac{\varepsilon_{xy}}{\varepsilon_{xx}} \sim \mathbf{M}$$

The above relation shows the origin of the small linear magneto-optical effects, which is the low magnitude of the magnetization-induced off-diagonal components of the dielectric tensor in comparison to the diagonal ones. We will see that this in not the case for the nonlinear magneto-optics, as detailed in the next section.

Depending on the involved MOKE geometry (see figure 3.5) one can map out the magnetization orientation in real space. For example in longitudinal geometry the in-plane magnetization can be probed, this characteristic being used in magnetic domains imaging. In polar configuration the projection of magnetization along z axis is determined, this geometry finds applications in magneto-optical recording [113]. Although MOKE is primarily a bulk sensitive technique since it averages over the optical penetration depth, one can resolve thicknesses in monolayer or even sub-monolayer range of a ferromagnetic material [114].

On a microscopic level, there is the combined effect of the spin-orbit coupling and the exchange interaction together with the selection rules for optical transitions that give rise to the observed magneto-optical effects. The optical transition in the electric-dipole approximation have different absorption probabilities for left and right circularly polarized light as can be seen in the figure 3.6. Writing the imaginary part of the non-diagonal component of conductivity tensor that determines the magneto-optical activity [115], one can identify on a microscopic scale the source of the magneto-optical effects:

$$\sigma^{"}_{xy}(\omega) = \frac{\pi e^2}{4\hbar\omega m^2\Omega} \sum_{i,f} f(E_i)[1-f(E_f)][|<i|p_-|f>|^2 - |<i|p_+|f>|^2]\delta(\omega_{fi}-\omega) \quad (3.28)$$

with *f(E)* representing the Fermi-Dirac function, $\hbar\omega$ being the energetic interval between the initial $|i>$ and final state $|f>$ and $\delta(\omega_{fi}-\omega)$ describing the energy conservation. If the difference between the matrix elements for dipole transitions corresponding to left $|<i|p_+|f>|$ and right $|<i|p_-|f>|$ circularly polarized light vanishes (the case of a paramagnet) than there is no net magneto-optical effect.
The above picture provides just a qualitative understanding regarding the origin of MO effects on a microscopic level. It was shown [116, 117] that is the change of the electronic wavefunctions due to the spin-orbit coupling rather than the energy eigenvalues shift which accounts for the proper order of magnitude of the MO effects.

3.3.2 Magnetization-induced second-harmonic generation

Previously we have discuss in detail the linear magneto-optical effects since these resemble several common features with, and are the basis for understanding of the nonlinear

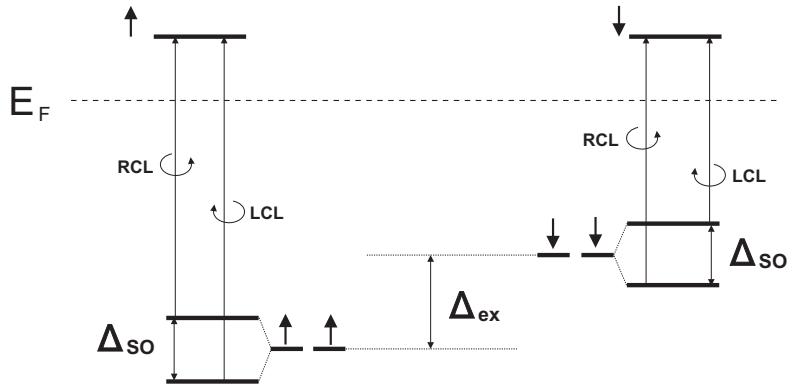

Figure 3.6: Microscopic picture of linear magneto-optical effects on a ferromagnetic material: the initial degeneracy of the ground electronic states is lifted by the presence of spin-orbit coupling while the exchange interaction produce a energetic shift Δ_{ex} of the electronic states with different spin orientation. The optical transitions for left (LCL) and right-handed (RCL) circularly polarized light evolve according to the selection rules $\Delta l = \pm 1$ and $\Delta m_l = \pm 1$. The overall effect is a different absorption probability for LCL and RCL that produces the rotation of polarization plane for the outgoing light [115].

magneto-optics, that is the topic of this section. Due to its linear optical character MOKE gives information about the magnetization behavior in the bulk region (within the optical penetration depth) of the materials. Although can reach atomic monolayer sensitivity [113, 114] of ferromagnetic films, MOKE lacks the surface or interface specificity.

Magnetization-induced second-harmonic generation, also known as the nonlinear magneto-optical Kerr effect (NOLIMOKE or NOMOKE), as a nonlinear optical process provides (within electric-dipole approximation) the surface and interface sensitivity (see preceding sections) and simultaneously gives a measure of the magnetization in the probed region. Similar to MOKE, the *MSHG is linear in magnetization* $\boldsymbol{M}$ *but is nonlinear in the optical field*. Beside these characteristics, MSHG can access buried interfaces of *e.g.* magnetic multilayered structures, with evident applications in magnetic data storage.

Although the SHG was first demonstrated in early 1960-ties [96], MSHG is a relatively young tool of investigation of ferromagnetic materials. The MSHG effects were first predicted in the theoretical work of Pan et al. [11], where it was shown that magnetization could induce a component of measurable magnitude to the total SHG response from a ferromagnetic material. The first experimental proof came from the work of Reif *et al.* [118] performed on the iron Fe(110) surface. Since then, the nonlinear magneto-optics field experienced a tremendous development which was partially triggered by the continuous interest in the physics of magnetic multilayered structures and their potential applications as well as the development of the ultrafast laser sources. The application range of MSHG covers a large spectrum starting from imaging of magnetic domains to investigation of spin dynamics on ultrafast time scales, and from investigation of spin reorientation transition of thin magnetic films to magnetic quantum wells. These are just a few examples that give a rough overview about the applicability of MSHG. For a better overview of the work done in this field, the reader is referred to the review of Kirilyuk [107].

As for the case of linear magneto-optics, the origin of the nonlinear magneto-optical effects rely on breaking of the time-reversal symmetry. In addition, breaking of space-inversion symmetry provides a high surface and interface sensitivity. These two symmetry considerations being fulfilled simultaneously, make the nonlinear magneto-optics in general and especially MSHG a very reliable investigation method of electronic and magnetic properties at surfaces and interfaces. Analogous to MOKE, in the case of MSHG the magnitude of the magnetization-induced effects is proportional to the ratio between the magnetic and non-magnetic tensor components *i.e.* odd and even with regard to magnetization reversal, respectively. Thus, both effects, MSHG and MOKE, resemble a similar feature namely are proportional with the magnetization of the investigated system. For the case of MOKE, the odd (off-diagonal) tensor components are usually small which explains the low magnitude effects encountered in linear magneto-optics. This is not the case of MSHG where the even and odd tensor components are of comparable magnitude, and therefore giving rise to much higher effects compared to linear magneto-optics. An illustrative example here is Ni, where for the same wavelength range, a ratio of the odd and even tensor components of 0.03 was found for linear magneto-optics whereas for the nonlinear magneto-optics a value of 0.27 was determined [117].

In general, for a ferromagnetic material the nonlinear source of the SH signal can be described by the second-order nonlinear polarization having the following form [107, 119]:

$$P_i^{(2)}(2\omega) = \chi_{ijk}^{(2)} E_j(\omega) E_k(\omega) + \chi_{ijkl}^{(3)} E_j(\omega) E_k(\omega) M_l \tag{3.29}$$

where the first term on the right-hand side describes the non-magnetic effects while the second is determined by the presence of magnetization. Defining [119] the magnetization-induced susceptibility tensor as:

$$\chi_{ijk}^{(2)}(M) \equiv \chi_{ijkl}^{(3)} M_l \tag{3.30}$$

one can express the susceptibility tensor giving rise to MSHG effects as a sum of second-order susceptibility components that behave even and odd with respect to magnetization reversal. Thus, one can write:

$$\chi_{ijk}^{(2)} = [\chi_{even}^{(2)}]_{ijk} + [\chi_{odd}^{(2)}(M)]_{ijk} \tag{3.31}$$

Experimentally one measures the SHG intensity for opposite magnetization directions, which can be written as:

$$I^{\uparrow\downarrow}(2\omega) \propto |E_{even}(2\omega) + E_{odd}(2\omega)|^2 \tag{3.32}$$

where $E_{even}(2\omega)$ and $E_{odd}(2\omega)$ are the even and odd SH fields generated by the nonlinear polarization described in eq. 3.29. The magnetization orientation is denoted by up and down arrows in the formula. Further on, the above equation becomes:

$$I^{\uparrow\downarrow}(2\omega) \propto |E_{even}(2\omega)|^2 + |E_{odd}(2\omega)|^2 \pm 2|E_{even}(2\omega)||E_{odd}(2\omega)| \cos\phi \tag{3.33}$$

where $\cos\phi$ represents the relative phase between the even and odd second harmonic fields. From here we see that the magnetization effects come from the cross term in the right-hand side of eq. 3.33, which gives the interference between the even and odd SH fields

and contains also their mutual phase ϕ. Hence, the phase between odd and even fields is a non-negligible quantity and should also evaluated from experiment. Its importance can be seen immediately by assuming a ϕ=90° value that gives a zero value for the cross term, which is equivalent with no magnetization-induced SHG signal. How to measure the relative phase between even and odd fields and the involved formalism will be presented in the chapter 5.

In this work we have used the transversal magneto-optical geometry in a p-P polarization configuration. This experimental geometry has been chosen since we are interested in the in-plane magnetization component (of ferromagnetic Gd(0001) films) and the highest number of even and odd tensor components contribute to the SHG response (see table 3.2). The latter fact ensures a high sensitivity of the SHG process to the magnetized medium through the cross term in eq 3.33. Also for the p-P geometry the magnitude of the Fresnel factors is higher that further enhances the SHG efficiency (see eq. 3.21).

In order to get information about the magnetization of the probed region, one can determine from the measured SH intensities the magnetic contrast or magnetic asymmetry. This is defined as the relative variations of the SHG intensity for opposite magnetization directions and it has the below form:

$$\rho = \frac{I^{\uparrow}(2\omega) - I^{\downarrow}(2\omega)}{I^{\uparrow}(2\omega) + I^{\downarrow}(2\omega)} \tag{3.34}$$

Taking into account the relation 3.33 one can write the magnetic contrast as:

$$\rho \approx 2\frac{|E_{odd}|}{|E_{even}|}\cos\phi \tag{3.35}$$

considering[2] that $\frac{|E_{odd}|}{|E_{even}|} \ll 1$. Since the magnetic contrast and the phase can be measured in the experiment, one can deduce the value of the even and odd SH fields. Moreover, accounting for the eq. 3.30 one obtains a direct relationship between the magnetic contrast and magnetization of the probed area:

$$\rho \approx 2\frac{|\chi^{(3)}_{odd}|}{|\chi^{(2)}_{even}|}M\cos\phi \tag{3.36}$$

Based on the above considerations, we can consider the magnetic contrast as a good measure of the magnetization in the probed region.

Time resolved MSHG

The measured observable in a time-resolved MSHG experiment is the intensity of second harmonic signal for opposite directions of magnetization and as a function of delay time between pump and probe beams. As has been shown previously, the SH intensity consists of even and odd fields with respect to magnetization reversal, which monitor [17] the electron (phonon) and spin subsystems, respectively. We are interested in the time evolution of the second-harmonic fields as a function of pump-probe delay. The first step

[2]The validity of the condition $\frac{|E_{odd}|}{|E_{even}|} \ll 1$ is demonstrated in chapter 5 for the case of Gd(0001) surface.

in their determination is computing the sum and difference of SHG intensities for opposite magnetic fields, accounting for eq. 3.33:

$$I^{\uparrow}(t) + I^{\downarrow}(t) = 2[E^2_{even}(t) + E^2_{odd}(t)] \tag{3.37}$$

$$I^{\uparrow}(t) - I^{\downarrow}(t) = 4E_{even}(t)E_{odd}(t)\cos\phi(t) \tag{3.38}$$

To deduce the transient SH fields, the ratios between the measured intensities for positive and negative time delays (in absence of the pump pulse) are computed under the form:

$$R(t)^{\pm} = \frac{I^{\uparrow}(t) \pm I^{\downarrow}(t)}{I^{\uparrow}(t_0) \pm I^{\downarrow}(t_0)} \tag{3.39}$$

In obtaining the upper expression in terms of transient SH fields we neglect the factor $|E_{odd}(2\omega)|^2$ since $|E_{odd}(2\omega)|^2 << |E_{even}(2\omega)|^2$ (as shown above). The resulting pump-induced variations in the second-harmonic fields are written as:

$$\frac{E_{even}(t)}{E_{even}(t_0)} = \sqrt{R^{+}(t)} \tag{3.40}$$

$$\frac{E_{odd}(t)cos\phi(t)}{E_{odd}(t_0)cos\phi(t_0)} = \frac{R^{-}(t)}{\sqrt{R^{+}(t)}} \tag{3.41}$$

The normalized ratio of the even field denote the dynamics of the electron system while the ratio of the odd fields gives measure of the magnetization dynamics in the probed region [17]. In the following, and throughout the thesis, the time-resolved SHG data will be presented under the following form:

$$\Delta_{even} = \sqrt{R^{+}(t)} - 1 \approx \frac{E_{even}(t)}{E_{even}(t_0)} - 1 \tag{3.42}$$

$$\Delta_{odd} = \frac{R^{-}(t)}{\sqrt{R^{+}(t)}} - 1 \approx \frac{E_{odd}(t)cos\phi(t)}{E_{odd}(t_0)cos\phi(t_0)} - 1 \tag{3.43}$$

Accounting for the expression 3.30 one can write the Δ_{odd} as [119]:

$$\Delta_{odd} \approx \alpha(t,\omega)\frac{M(t)}{M(t_0)} - 1 \tag{3.44}$$

with the prefactor defined as:

$$\alpha(t,\omega) \equiv \frac{\chi^{(3)}_{odd}(t)}{\chi^{(3)}_{odd}(t_0)} \cdot \frac{cos\phi(t)}{cos\phi(t_0)} \tag{3.45}$$

From the above equations we notice that Δ_{odd} measures the transient magnetization of the system multiplied by a factor that depends on the relative phase between the SH fields and the normalized ratio of the third-order susceptibility. In principle one can measure the relative phase in a time-resolved manner. For the case of Gd(0001) such measurements

are hindered by the relatively low SHG signal and the inherent technical difficulty of measuring SHG phase in UHV. However, spectroscopic measurements of the phase [119] (see chapter 5) in the static case performed on Gd(0001) yield a value $\phi < 20°$ that gives $\cos\phi(t_0) \approx 1$. Time-resolved MSHG measurements performed on Ni samples in air [120] showed the pump-induced variations of the phase to be small and consequently $\frac{\cos\phi(t)}{\cos\phi(t_0)} \approx 1$. Accounting for the Ni experiment and since for the Gd(0001) surface $\cos\phi(t_0) \approx 1$ we can conclude that $\frac{\cos\phi(t)}{\cos\phi(t_0)} \approx 1$ is valid for time-resolved MSHG measurements performed on Gd(0001). From the spectroscopic behavior of the Δ_{odd} and Δ_{even} we deduce a minor role of the susceptibility ratio in the dynamics of Δ_{odd} [119]. Thus, we can conclude that the quantity Δ_{odd} reflects, mostly, the dynamics of the surface magnetization.